

A Standardized Pipeline for Examining Human Cerebellar Grey Matter Morphometry using Structural Magnetic Resonance Imaging

Rebecca Kerestes¹, Shuo Han², Srinivas Balachander³, Carlos Hernandez-Castillo⁴, Jerry L. Prince^{5,6}, Jörn Diedrichsen⁷, Ian H. Harding^{1,8}

¹ Department of Neuroscience, Central Clinical School, Monash University ² Department of Biomedical Engineering, The Johns Hopkins University ³ Department of Psychiatry, National Institute of Mental Health & Neuro Sciences (NIMHANS) ⁴ Faculty of Computer Science, Dalhousie University ⁵ Department of Electrical and Computer Engineering, The Johns Hopkins University ⁶ Department of Computer Science, The Johns Hopkins University ⁷ Brain and Mind Institute, Department for Statistical and Actuarial Sciences, Department for Computer Science, Western University ⁸ Monash Biomedical Imaging, Monash University

Corresponding Author

Rebecca Kerestes
rebecca.kerestes@monash.edu

Citation

Kerestes, R., Han, S., Balachander, S., Hernandez-Castillo, C., Prince, J.L., Diedrichsen, J., Harding, I.H. A Standardized Pipeline for Examining Human Cerebellar Grey Matter Morphometry using Structural Magnetic Resonance Imaging. *J. Vis. Exp.* (), e63340, doi:10.3791/63340 (2022).

Date Published

February 3, 2022

DOI

10.3791/63340

URL

jove.com/t/63340

Abstract

Multiple lines of research provide compelling evidence for a role of the cerebellum in a wide array of cognitive and affective functions, going far beyond its historical association with motor control. Structural and functional neuroimaging studies have further refined understanding of the functional neuroanatomy of the cerebellum beyond its anatomical divisions, highlighting the need for the examination of individual cerebellar subunits in healthy variability and neurological diseases. This paper presents a standardized pipeline for examining cerebellum grey matter morphometry that combines high-resolution, state-of-the-art approaches for optimized and automated cerebellum parcellation (Automatic Cerebellum Anatomical Parcellation using U-Net Locally Constrained Optimization; ACAPULCO) and voxel-based registration of the cerebellum (Spatially Unbiased Infra-tentorial Template; SUIT) for volumetric quantification.

The pipeline has broad applicability to a range of neurological diseases and is fully automated, with manual intervention only required for quality control of the outputs. The pipeline is freely available, with substantial accompanying documentation, and can be run on Mac, Windows, and Linux operating systems. The pipeline is applied in a cohort of individuals with Friedreich ataxia (FRDA), and representative results, as well as recommendations on group-level inferential statistical analyses, are provided. This pipeline could facilitate reliability and reproducibility across the field, ultimately providing a powerful methodological approach for characterizing and tracking cerebellar structural changes in neurological diseases.

Introduction

The cerebellum is a part of the brain historically associated with motor control^{1,2,3} and is thought to be integrally involved in only a small set of rare diseases, such as inherited ataxias⁴. However, converging lines of research from anatomical tracing studies in nonhuman primates, as well as human lesion and neuroimaging studies, provide compelling evidence for a role of the cerebellum in a wide array of cognitive^{5,6,7}, affective^{8,9,10,11}, and other nonmotor functions^{7,12} (see⁶ for review). Furthermore, abnormalities of the cerebellum are increasingly implicated in a broad range of neurological and psychiatric disorders, including Parkinson's disease¹³, Alzheimer's disease^{14,15}, epilepsy^{16,17}, schizophrenia¹⁸, and autism spectrum disorder¹⁹. Therefore, it has become essential to incorporate the cerebellum into functional and structural models of human brain diseases and normative behavioral variability.

Anatomically, the cerebellum can be divided along its superior to inferior axis into three lobes: anterior, posterior, and flocculonodular. The lobes are further subdivided into 10 lobules denoted by roman numerals I-X^{20,21} (**Figure 1**). The cerebellum can also be grouped into midline (vermis) and lateral (hemisphere) zones, which respectively receive inputs from the spinal cord and cerebral cortex. The anterior lobe, comprising lobules I-V, has traditionally been associated with motor processes and has reciprocal connections with cerebral motor cortices²². The posterior lobe, comprising lobules VI-IX, is primarily associated with nonmotor processes¹¹ and has reciprocal connections with the prefrontal cortex, posterior parietal, and superior temporal cerebral cortices^{8,23}. Lastly, the flocculonodular lobe, comprising lobule X, has reciprocal connections with

vestibular nuclei that govern eye movements and body equilibrium during stance and gait²¹.

A growing body of recent work using functional neuroimaging has further refined understanding of the functional neuroanatomy of the cerebellum beyond its anatomical divisions. For example, resting-state functional magnetic resonance imaging (fMRI) techniques have been used to map the pattern of functional interactions between the cerebellum and cerebrum²⁴. Additionally, using a task-based parcellation approach, King and colleagues⁷ demonstrated that the cerebellum shows a rich and complex pattern of functional specialization across its breadth, evidenced by distinct functional boundaries associated with a variety of motor, affective, social, and cognitive tasks. Collectively, these studies highlight the importance of examining individual cerebellar subunits to develop complete biological characterizations of cerebellum involvement in both healthy variability and neurological diseases characterized by alterations in cerebellar structure and/or function.

The present work focuses on methods for quantifying local changes in cerebellar volume using structural MRI in humans. In general, there are two fundamental approaches to the quantification of regional brain volume using MRI data: feature-based *segmentation* and *voxel-based registration*. Feature-based segmentation approaches use anatomical landmarks and standardized atlases to automatically identify boundaries between subregions. Mainstream software packages for segmentation include FreeSurfer²⁵, BrainSuite²⁶, and FSL-FIRST²⁷. However, these packages provide only coarse parcellations of the cerebellum (e.g., labeling the whole grey matter and whole

white matter in each hemisphere), thus overlooking the individual cerebellar lobules. These approaches are also prone to mis-segmentation, particularly overinclusion of the surrounding vasculature.

New machine-learning and multi-atlas labeling algorithms have been developed, which provide more accurate and finer-grained parcellation of the cerebellum, including Automatic Classification of Cerebellar Lobules Algorithm using Implicit Multi-boundary evolution (ACCLAIM^{28,29}), Cerebellar Analysis Toolkit (CATK³⁰), Multiple Automatically Generated Templates (MAGeT³¹), Rapid automatic segmentation of the human cerebellum and its lobules (RASCAL³²), graph-cut segmentation³³, and CEREBellum Segmentation (CERES³⁴). In a recent paper comparing state-of-the-art fully automated cerebellum parcellation approaches, CERES2 was found to outperform other approaches relative to gold-standard manual segmentation of the cerebellar lobules³⁵. More recently, Han and colleagues³⁶ developed a deep-learning algorithm called ACAPULCO (Automatic Cerebellum Anatomical Parcellation using U-Net with locally constrained optimization), which performs on par with CERES2, has broad applicability to both healthy and atrophied cerebellums, is available in open-source Docker and Singularity container format for 'off-the-shelf' implementation, and is more time-efficient than other approaches. ACAPULCO automatically parcellates the cerebellum into 28 anatomical regions.

In contrast to feature-based segmentation, voxel-based registration approaches operate by precisely mapping an MRI to a template image. To achieve this mapping, the voxels in the original image must be distorted in size and shape. The magnitude of this distortion effectively provides a measure of volume at each voxel relative to the gold-standard template. This form of volumetric assessment is known as 'voxel-

based morphometry'³⁷. Whole-brain voxel-based registration approaches, such as FSL-FLIRT³⁸/FNIRT³⁹, SPM unified segmentation⁴⁰, and CAT12⁴¹, are commonly used for voxel-based morphometry. However, these approaches do not account well for the cerebellum, resulting in poor reliability and validity in infratentorial regions (cerebellum, brainstem⁴²). To account for these limitations, the SUIT (Spatially Unbiased Infra-tentorial Template) algorithm was developed to optimize cerebellum registration and improve the accuracy of voxel-based morphometry^{42,43}.

Feature-based segmentation and voxel-based registration approaches for the estimation of regional cerebellar volume have fundamental strengths and weaknesses. Segmentation approaches are substantially more accurate for quantifying the volume of anatomically defined areas (e.g., lobules³⁵). However, boundaries between distinct functional modules of the cerebellum do not map onto its anatomical folia and fissures (equivalent to gyri and sulci of the cerebrum⁷). As registration-based approaches are not constrained by anatomical landmarks, finer-grained spatial inference and high dimensional structure-function mapping of the cerebellum is possible⁴⁴. Taken together, segmentation and registration approaches are complementary to one another and can be used to answer different research questions.

Here, a new standardized pipeline is presented, which integrates these existing, validated approaches to provide optimized and automated parcellation (ACAPULCO) and voxel-based registration of the cerebellum (SUIT) for volumetric quantification (**Figure 2**). The pipeline builds upon the established approaches to include quality control protocols, using qualitative visualization and quantitative outlier detection, and a rapid method for obtaining an estimation of intracranial volume (ICV) using Freesurfer. The

pipeline is fully automated, with manual intervention only required for checking the quality control outputs, and can be run on Mac, Windows, and Linux operating systems. The pipeline is freely available with no restrictions of its use for noncommercial purposes and can be accessed from the ENIGMA Consortium Imaging Protocols webpage (under "ENIGMA Cerebellum Volumetrics Pipeline"), following the completion of a brief registration form⁴⁵.

All required software is listed in the **Table of Materials**, and detailed tutorials, including a live demonstration, are available upon download of the pipeline, in addition to the protocol described below. Finally, representative results are provided, from the implementation of the pipeline in a cohort of people with Friedreich ataxia (FRDA) and age- and sex-matched healthy controls, alongside recommendations for group-level statistical inferential analyses.

Protocol

NOTE: The data used in this study were part of a project approved by the Monash University Human Research Ethics Committee (project 7810). Participants provided written informed consent. While the pipeline can be run on Mac, Windows, or Linux operating systems, ACAPULCO, SUIT, and the QC pipelines have explicitly been tested on Linux (Ubuntu) and Mac (Catalina, Big Sur v11.0.1) operating systems.

1. Module 1: ACAPULCO (anatomical parcellation)

1. Data collection

1. Collect 3D T1-weighted MRI images of the whole brain at a resolution of 1 mm³ or less. Isotropic voxel dimensions (typically 1 mm x 1 mm x 1 mm), and a 3-Tesla (or greater) scanner are

recommended. Consult with an imaging specialist at their radiography center to set up and acquire data that meet these specifications.

NOTE: T2-weighted images are sometimes useful for volumetric analyses; however, the pipeline presented here relies on T1-weighted data only, and some of the tools used are exclusive to this type of data. As such, T2-weighted images cannot be used.

2. Undertake a visual quality assessment of images to exclude gross cerebellar malformations (e.g., large lesions) or substantial motion artifacts that prevent identification of major cerebellar landmarks (e.g., the major anatomical fissures). Do not automatically exclude atrophied cerebella, even if substantial.
 3. For group studies, also consider quantitative quality assessments using freely-available, standardized tools such as MRIQC⁴⁶ to further identify problematic data.
 4. Convert all data to NIFTI-GZ format using a tool such as dcm2niix⁴⁷.
- #### 2. Recommended data organization
1. Obtain all necessary software as listed in the **Table of Materials**. Ensure Docker⁴⁸ or Singularity⁴⁹, Matlab⁵⁰, and SPM12⁵¹ are installed prior to running the pipeline.

NOTE: Extensive written and video tutorials describing the pipeline are also available (see the **Table of Materials**).
 2. Once all necessary software is installed, create folders in the working directory and label them 'acapulco,' 'suit,' and 'freesurfer.' Do this using the **mkdir** command from the command line.

3. In the 'acapulco' directory, create an **output** folder. In the **output** folder, create a directory for each subject in the study containing the T1-weighted image in NIFTI-GZ format.

NOTE: It is recommended to keep a copy of the original data elsewhere.

3. Anatomical cerebellar parcellation using ACAPULCO

1. Go to the **Table of Materials** and download the relevant scripts and containers required to run ACAPULCO (under **acapulco pipeline files**). In the 'acapulco' directory, place the (i) ACAPULCO Docker OR Singularity container ('acapulco_0.2.1.tar.gz' or '.sif', respectively), (ii) contents of the QC_scripts archive (3 files: 'QC_Master.R,' 'QC_Plots.Rmd,' and 'QC_Image_Merge.Rmd'), and (iii) 'R.sif' (singularity) OR 'calculate_icv.tar' (docker) file.
2. Open a terminal, and from the command line, run the ACAPULCO container on a single image (replace <<subject>> in the following). Wait for ~5 min for processing to complete.

1. Using Docker, type the command:

```
docker load --input acapulco_0.2.1.tar.gz
docker run -v $PWD:$PWD -w $PWD -t
--user $(id -u):$(id -g) --rm acapulco:latest
-i output/<<subject>>/<<subject>>.nii.gz -o
output/<<subject>>
```

2. Using Singularity, type the command:

```
singularity run --cleanenv -B $PWD:
$PWD acapulco-0.2.1.sif -i output/<<subject>>/
<<subject>>.nii.gz -o output/<<subject>>
```

3. Loop across all subjects/scans in the cohort. See the **Table of Materials** for a link to the ENIGMA

Imaging Protocols website for downloading the pipeline (under **ENIGMA Cerebellum Volumetrics Pipeline**) and the tutorial manual containing examples of how to create a for-loop for processing multiple subjects serially.

4. After processing, look for the following files generated in the subject-specific folders:

1. Identify

"<subject>_n4_mni_seg_post_inverse.nii.gz":
parcellated cerebellum mask in original (subject space).

2. Identify

"<subject>_n4_mni_seg_post_volumes.csv":
volumes (in mm³) for each of the 28 subunits generated by acapulco;

3. Identify representative images (in 'pics' directory): sagittal, axial, and coronal.

4. Statistical outlier detection and quality control (QC)

1. From the terminal and in the 'acapulco' directory, ensure that the contents of QC_scripts are in the 'acapulco' directory. To run the QC scripts:

1. Using Docker, type the command:

```
docker load calculate_icv.tar
docker run -v $PWD:$PWD -w $PWD --rm -it
luhancheng/calculate_icv:latest Rscript
QC_Master.R output/
```

2. Using Singularity, type the command:

```
singularity exec -B $PWD:$PWD R.sif Rscript /
path/to/QC_Master.R /path/to/acapulco/output
```

5. Examining the QC images generated by ACAPULCO

NOTE: There is a 3-step process for quality checking the ACAPULCO parcellated images.

1. Open the 'QC_Images.html' in a web browser and quickly (~10 s per subject) scroll through the images to identify obvious failures or systematic issues. Note the subject IDs of failed or suspect parcellated images for follow-up.

NOTE: See **Figure 3** for a guide on the neuroanatomy of the cerebellar lobules and **Figure 4**, **Figure 5**, and **Figure 6** in the representative results section below for examples of 'good' parcellations, 'subtle mis-parcellations,' and 'global failure' parcellations.

2. Open the 'Plots_for_Outliers.html' to check the boxplots for quantitative statistical outliers. Look for outliers (2.698 s.d above or below the mean) above or below the whiskers of the box plots. Hover over the data points to display the Subject ID. Identify the outliers denoted by a '1' in the relevant column in the 'Outliers.csv' file, and note the total number of segments identified as outliers for each subject in the final column in 'Outliers.csv.'

3. Manually inspect each image having one or more outliers. **CRITICAL:** Using a standard NIFTI image viewer (e.g., FSLEyes or MRICron), overlay the ACAPULCO mask onto the original T1w image to check the quality of the parcellation slice-by-slice.

1. To generate overlays for detailed QC from the command line using FSLEyes, i) change the directory to the 'acapulco' directory, ii) specify the subject to view (replace *<subject>*):

```
subj=<subject_name>
```

2. Copy/paste the following code to the terminal (without manually changing {subj}) as this has been set by the previous line:

```
t1_image=output/${subj}/${subj}.nii.gz
acapulco_image=output/${subj}/
${subj}_n4_mni_seg_post_inverse.nii.gz
fsleyes ${t1_image} ${acapulco_image}
--overlayType label --lut random_big --
outline --outlineWidth 3 ${acapulco_image} --
overlayType volume --alpha 50 --cmap random
```

NOTE: A determination will need to be made whether to include the abnormal segment or not, i.e., is there a parcellation error, or is it just normal variability in the individual's anatomy? Each parcellated region is considered individually, so a few regions can be excluded for an image, while the remainder can be retained if correct.

3. *Do one or more parcellated regions need to be excluded from the final dataset?*

If Yes (outlier is confirmed), exclude this parcellation(s) from the analysis by replacing the volume estimate with **NA** in the corresponding cell of the 'Cerebel_vols.csv' file for that subject.

4. *Do parcellation errors result in some of the cerebellum being excluded from the mask?*

If Yes, (for example, if particular cerebellar lobules are missing from the mask or appear 'cut off'), immediately exclude the subject from further analyses (i.e., do not proceed to run the SUIT module on those subjects).

2. Module 2: SUIT cerebellum-optimized voxel-based morphometry

1. Voxel-based morphometry analyses using SUIT

CRITICAL: This pipeline requires the ACAPULCO module to have already been run, as it relies on the generation of a subject-specific cerebellar mask for optimization of the registration and normalization of the cerebellum to the SUIT template. If the subject-specific mask generated by ACAPULCO does not include the whole cerebellum, this warrants exclusion from the SUIT module. For instructions on running SUIT standalone, see⁵².

1. Obtain all necessary software listed in the **Table of Materials**. Ensure the SPM12 folder and all subfolders are in the MATLAB path. Ensure `enigma_suit` scripts are saved in 'spm12/toolbox' directory and added to the MATLAB path. To check the MATLAB path, type `pathtool` in the MATLAB command window, then click **Add with subfolders** to add the relevant folders.
2. Run the SUIT pipeline for one or more subjects. Wait for ~15-20 min (if using the graphical user interface [GUI]) and ~5-7 min if running from the terminal (bash/shell) for processing to complete.
 1. To use the GUI (subjects will be run in serial), from the MATLAB command window, type the command:
`suit_enigma_all`
 2. In the first pop-up window, select the subject folders from the 'acapulco/output' directory to include in the analysis. Click on the individual folders on the right side of the window, or right-click and **Select All**. Press **Done**. In the second pop-up window, select the SUIT directory, where the analyses will be written.

3. OR Call the function from the MATLAB command line for a single subject, type the command:

```
suit_enigma_all('/path/to/acapulco/output/  
subjdir','/path/to/suitoutputdir')
```

4. OR Call the function from the terminal window, outside of MATLAB, for a single subject by typing the command:

```
matlab -nodisplay -nosplash -  
r "suit_enigma_all('/path/to/acapulco/output/  
subjdir','/path/to/suitoutputdir'), exit"
```

3. See the **Table of Materials** for a link to the ENIGMA Imaging Protocols website for downloading the pipeline (under **ENIGMA Cerebellum Volumetrics Pipeline**) and the tutorial manual containing examples of how to create a for-loop for processing multiple subjects serially.
4. Look for the following points regarding the script.
 1. Ensure that the script copies the N4 bias-corrected, MNI-aligned (rigid-body) T1 image and the ACAPULCO cerebellum mask into the output directory.
 2. Ensure that the script segments the grey and white matter of the cerebellum.
 3. Ensure that the script corrects for overinclusion errors in the parcellation using the ACAPULCO mask.
 4. Ensure that the script DARTEL normalizes and reslices the data into SUIT space with Jacobian modulation so that the value of each voxel is proportional to its original volume.

5. Check each subject's folder for the following final outputs: 'wd<subject>_seg1.nii' (grey matter) and 'wd<subject>_seg2.nii' (white matter).

2. Statistical outlier detection and quality control

1. Visually inspect the normalized, modulated images (wd*) for major failures. In MATLAB, type the command:

```
spm_display_4D
```

2. Manually select the 'wd*seg1' images from the suit subfolders, or navigate to the 'suit' directory; insert '^wd.*seg1' in the Filter box (no quotations) and press **Rec** button. Press **Done**.

3. Scroll through the images to ensure they are all well-aligned. See **Figure 7** for correctly normalized images from healthy controls (**A,B**) and an individual with a heavily atrophic cerebellum (**D**).

NOTE: At this stage, the between-subject anatomy is very similar (as they have been registered to the same template), and volume differences are instead encoded by differing voxel intensities. Major failures will be obvious, e.g., blank images, large areas of missing tissue, unusual intensity gradients (i.e., bright voxels all at the top, dark voxels all at the bottom). These images should be excluded from subsequent steps.

4. Check spatial covariance for outliers. In MATLAB, type the command:

```
check_spatial_cov
```

1. Select the 'wd*seg1' images as per the previous step. When prompted, select the following options: **Prop scaling: Yes; Variable to covary out: No; Slice (mm): - 48 , Gap: 1.**

2. Look at the boxplot displaying the mean spatial covariance of each image relative to all others in the sample. Identify data points that are >2s.d. below the mean in the MATLAB command window. For these, inspect the "<subj>_n4_mni.nii.gz" image in the SUIT folder for artifacts (motion, anatomical abnormalities), image quality issues, or preprocessing errors.
3. If the image quality and preprocessing are acceptable and visual inspection of the modulated images in the previous step does not indicate an issue with segmentation and normalization, retain these data in the sample. Otherwise, exclude these data.

3. MODULE 3 (optional): Intracranial Volume (ICV) estimation using FreeSurfer

NOTE: This module will use the FreeSurfer pipeline to calculate ICV. It does not need to be re-run if there are existing Freesurfer outputs for the cohort (any version).

1. Setting up FreeSurfer

1. Ensure FreeSurfer is downloaded and installed⁵³. Go to the **Table of Materials** and download the relevant scripts to run this Module (under **ICV pipeline files**). When working with FreeSurfer, set the following variables:

```
export
```

```
FREESURFER_HOME=<freesurfer_installation_directory>
```

```
source $FREESURFER_HOME/
```

```
SetUpFreeSurfer.sh
```

2. Replace **<path>** in the following:

```
export SUBJECTS_DIR=<path>/enigma/Freesurfer
```


2. Running Freesurfer autorecon1

1. For a single subject, from inside the 'freesurfer' directory (processing time ~20 min), type the command:

```
cd <path>/enigma/freesurfer
recon-all -i ../input/<subject>.nii.gz -s <subject> -
autorecon1
```

2. See the tutorial manual for examples of how to create a for-loop for processing multiple subjects serially.

3. Calculation of ICV

1. Data organization

1. In the 'freesurfer' directory, place the (i) Docker OR Singularity container used in Module 1 ('calculate_icv.tar' or 'R.sif,' respectively) and (ii) xfm2det script (see the **Table of Materials**). Then, do a git clone to clone the required ICV script:

```
git clone https://github.com/Characterisation-
Virtual-Laboratory/calculate_icv
```

2. Running ICV extraction (processing time ~5 min)

1. From 'freesurfer' directory, with singularity ('R.sif') container, type:

```
singularity exec --cleanenv -B $PWD:
$PWD R.sif calculate_icv/calculate_icv.py --
freesurfer_dir=/path/to/freesurfer --
acapulco_dir=/path/to/acapulco/QC/
Cerebelvolsfile --
output_csv_name=Cerebel_vols.csv
calculate_icv
```

2. From 'freesurfer' directory, with docker container, type:

```
docker run -v $PWD:$PWD -w $PWD -rm -it
luhancheng/calculate_icv:latest
calculate_icv/calculate_icv.py --
freesurfer_dir=/path/to/Freesurfer --
acapulco_dir=/path/to/acapulco/QC/
Cerebelvolsfile --
output_csv_name=Cerebel_vols.csv
calculate_icv
```

3. Running script without container-see the **Table of Materials** for additional required software and dependencies. From the 'freesurfer' directory, type:

```
./calculate_icv/ calculate_icv.py ---
freesurfer_dir=/path/to/freesurfer --
acapulco_dir=/path/to/acapulco/QC/
Cerebelvolsfile --
output_csv_name=Cerebel_vols.csv
calculate_icv
```

NOTE: This will calculate the ICV for each subject and append a column with ICV to the end of the 'Cerebel_vols.csv' file.

Representative Results

Cerebellum parcellation (ACAPULCO)

Quality control of cerebellum parcellated masks:

The following examples demonstrate the ACAPULCO parcellated outputs and guide decision-making about a) the quality of the parcellated mask at the individual level and b) subsequent inclusion or exclusion of a particular lobule(s) from the statistical analyses. Ultimately, the decision to include or exclude a subject is subjective; examples of 'good parcellations,' 'subtle parcellation errors,' and 'global failures' from a variety of healthy and clinical groups are provided here.

Examples of 'good parcellations' are presented in **Figure 4**, including in healthy and heavily atrophied cerebella. In **Figure 5**, subtle over- and under-inclusions of individual cerebellum lobules are depicted. These are the most common type of parcellation error and may not be detected as statistical outliers in the quantitative QC protocol. These types of errors generally require the exclusion of the individual lobules that are affected, while the remainder of the parcellated cerebellum is unaffected and can be retained. In contrast, 'Global failures,' as depicted in **Figure 6**, require complete exclusion of the subject.

Statistical outlier detection:

To illustrate the pipeline, ACAPULCO was run on a sample of 31 people with FRDA (mean age= 36.5 years; SD= 13.0 years, 14 females) and 37 age- and sex-matched healthy controls (HC) (mean age= 37.1 years; SD=12.8 years, 17 females) as previously described⁵⁵. Across the whole sample, 18 lobules were detected as statistical outliers (<1% of the total sample). After performing detailed QC on the images, 17 outlier lobules were removed from group-level analyses by removing the individual lobule volume for the respective subject(s) from the group-level cerebellar volumes file (i.e., the 'Cerebel_vols.csv' file). The remaining outlier was deemed not a segmentation error but rather due to variability in the individual's cerebellum anatomy and was therefore retained in the analysis. There were also two global parcellation failures (1 FRDA patient). The base rate of exclusion across all cerebellum lobules (i.e., global parcellation failures) was 1.5%. **Table 1** shows the exclusion rates for each of the 28 anatomical ROIs. Left lobule IX and Right lobule Crus I had the highest rates of exclusion.

Group-level statistical analysis:

A total of 66 subjects (30 FRDA patients) were included in the group-level analysis. Two-tailed Mann-Whitney independent samples tests were conducted to test for significant differences in cerebellum lobule volumes between FRDA and HC. Results showed significantly reduced white matter in the corpus medullare in FRDA vs. HC ($p < 0.05$, Bonferroni corrected for 28 comparisons). There were no other significant between-group differences. See **Supplemental Table S1** for the volumes of all 28 cerebellar subunits in the sample.

Cerebellum voxel-based morphometry analyses (SUIT)

Quality control:

Examples of well-aligned images and examples of exclusions for both healthy controls and clinical groups, including FRDA and Spinocerebellar ataxia patients, are shown in **Figure 7**. SUIT analyses were run on a total of 64 subjects (28 FRDA; 36 HC) from the sample described above, following the exclusion of an additional two subjects due to incomplete whole cerebellar coverage in the cerebellum mask.

After testing the spatial covariance of all normalized images in the sample relative to each other, two scans were detected as statistical outliers based on their mean spatial covariance with the rest of the sample (**Figure 8**). However, visual inspection of both the original and normalized images indicated that although these individuals had some unique neuroanatomy, there were no significant artifacts in either image and the processing steps completed normally. As such, both subjects were retained in the analyses.

Group-level statistical analysis:

Images were smoothed using a Gaussian kernel of 3 mm full width at half maximum (FWHM). Nonparametric permutation tests were carried out in SnPM to test for significant between-

group differences in cerebellum grey matter volumes. To this end, 5,000 permutations were run, with a cluster-forming threshold of $p < 0.001$. Images were explicitly masked with the SUIT grey matter atlas to limit inference to grey matter regions. To correct for head size, intracranial volume was entered as a covariate in the model. Final inference of group results was carried out at $p < 0.05$, family-wise error (FWE) cluster-level corrected.

Compared to HC, FRDA showed significantly reduced grey matter volume in bilateral anterior lobules I-V (left: $x = -10, y = -46, z = -26; T = 5.61; Ke = 754$; right: $x = 10, y = -38, z = -21; T = 6.83; Ke = 569$); and in medial posterior lobe regions, including Vermis VI, extending bilaterally into Lobule VI ($x = 3, y = -65, z = -20; T = 7.25$), and Vermis IX extending bilaterally into Lobule IX ($x = 3, y = -65, z = -20; T = 6.46; Ke = 3974$; **Figure 9**).

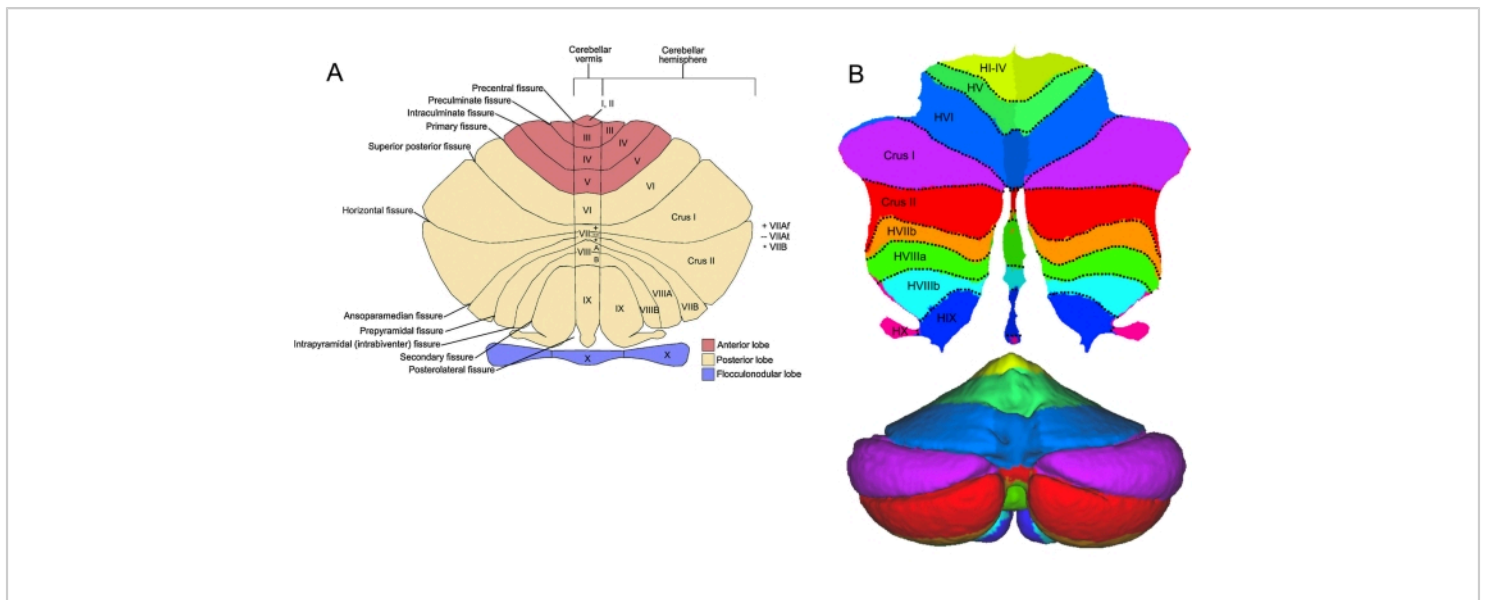


Figure 1: The human cerebellum. (A) A flattened representation of the cerebellum and its major fissures, lobes, and lobules. Red = anterior lobe (lobules I-V); cream= posterior lobe (lobules IV-IX); purple= flocculonodular lobe. The cerebellum can be divided into midline "vermis" and lateral "hemisphere" zones. All lobules are identified in the vermis and hemispheres. In lobule VII, VIIAf in the vermis expands in the hemispheres to become Crus I, lobule VIIAt at the vermis becomes Crus II in the hemispheres, and lobule VIIB retains its label both in the vermis and hemispheres. (B) Top: Cerebellum flat map showing the anatomical subunits of the cerebellum in different colors. Bottom: a posterior view of the cerebellum. This figure was adapted from ⁵⁶ and ⁵⁷. [Please click here to view a larger version of this figure.](#)

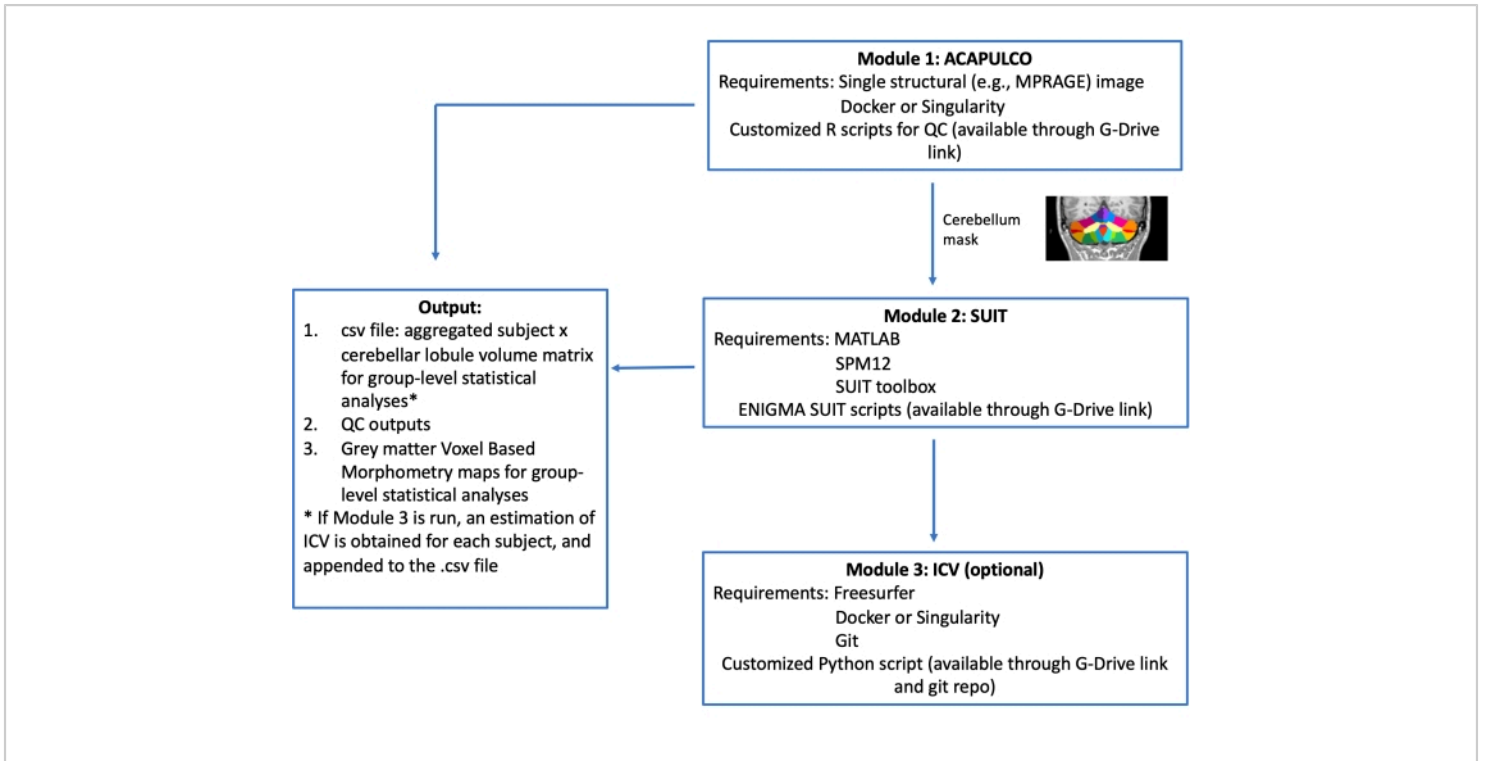


Figure 2: Schematic illustration of the pipeline. A high-resolution T1 MPRAGE image is required. There are three modules: ACAPULCO, SUIT, and ICV. The pipeline is fully automated (except for manual intervention required for QC of the outputs), is available in Docker and Singularity container format, and takes approximately 20 min to run from start to finish, per subject. [Please click here to view a larger version of this figure.](#)

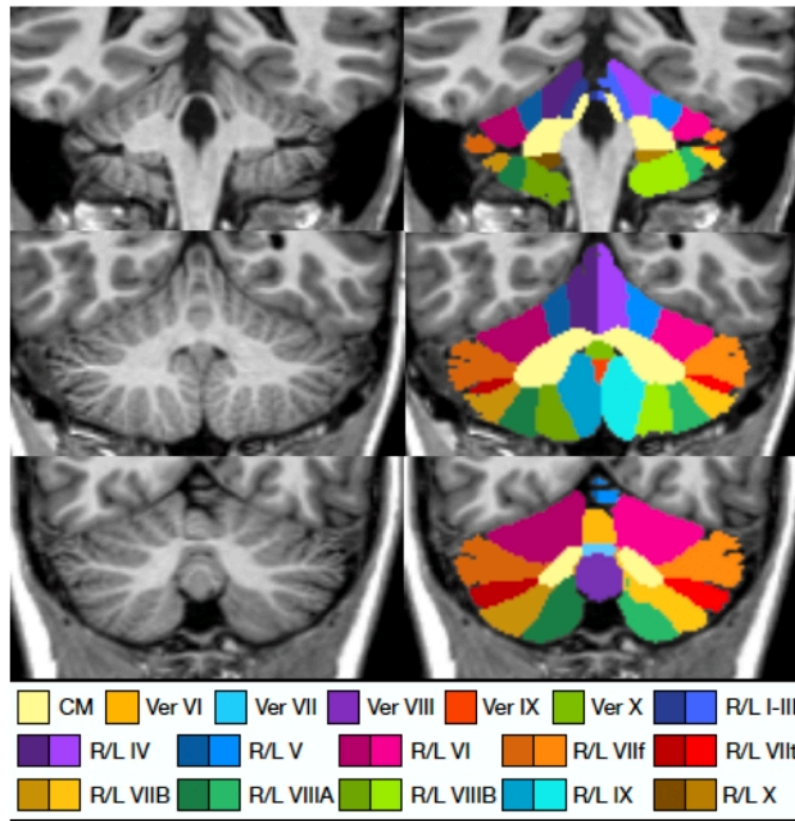


Figure 3: ACAPULCO parcellation demonstrating each of the 28 anatomical subunits. This figure was adapted from³⁶. Abbreviations: CM = corpus medullare; Ver = vermis; R/L = right/left. [Please click here to view a larger version of this figure.](#)

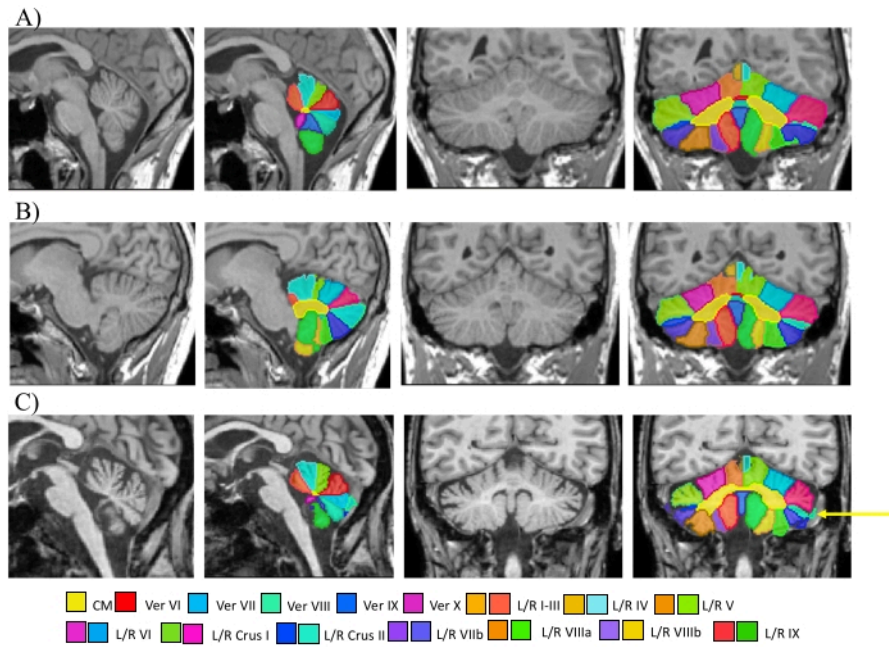


Figure 4: Examples of 'good' cerebellum parcellations. Sagittal ($x=0$) and coronal ($y=-57$) slices are shown. **(A, B)** Sagittal and coronal slices showing parcellated masks from two healthy cerebellar. The algorithm has localized the individual subunit boundaries correctly, and it has not overincluded the transverse sinus into the labeling and quantification of Crus I. **(C)** A heavily atrophied cerebellum of a SCA2 patient. Here, atrophy is apparent along the entire extent of the cerebellum, the sulci are broad, and there is a lot of missing tissue. There is a slight overinclusion of the vasculature in the posterior lobes that is more pronounced on the right side (yellow arrow). Aside from this overinclusion, ACAPULCO has worked well. Abbreviations: CM = corpus medullare; Ver = vermis; L/R = left/right. [Please click here to view a larger version of this figure.](#)

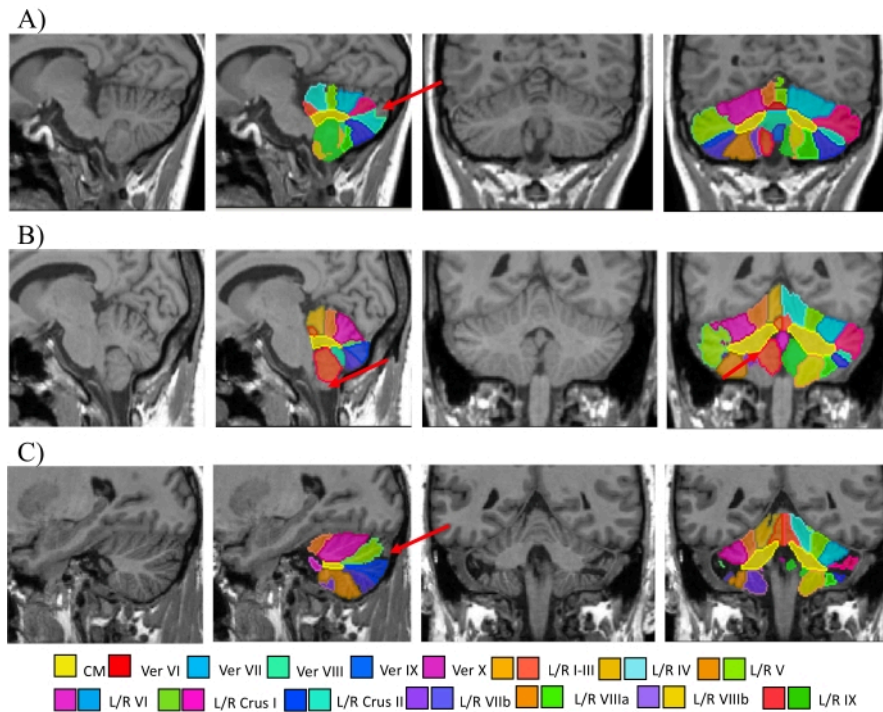


Figure 5: Examples of cerebellar 'mis parcellations.' (A) Sagittal slice ($x= 0$) and coronal slice ($y = -57$) showing a parcellation error in an FRDA patient. The algorithm has not worked well along the midline, and underinclusions of Crus I and II (red arrow) are evident along the posterior extent. These lobules would be excluded from subsequent group-level analyses. (B) Sagittal slice ($x= 8$), coronal slice ($y= -47$) showing a parcellation error in a healthy cerebellar. The algorithm has completely missed left lobule VIIIb (red arrows). This lobule would be excluded from subsequent group-level analyses. (C) Sagittal slice ($x= -24$) and coronal slice ($y= -47$) showing a parcellation error in a healthy cerebellar. Some cerebellar atrophy is present, and there is an underinclusion of Crus I (red arrow). Abbreviations: FRDA = Friedreich ataxia; CM = corpus medullare; Ver = vermis; L/R = left/right. [Please click here to view a larger version of this figure.](#)

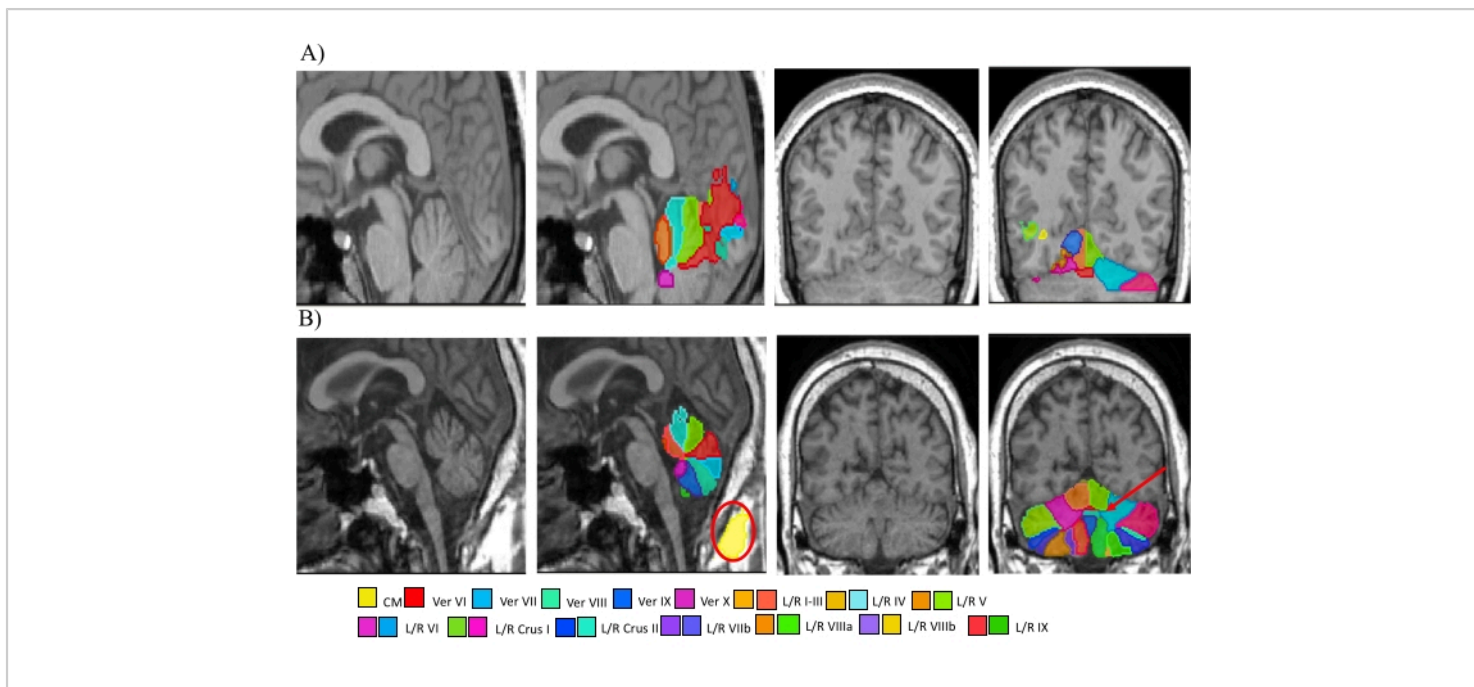


Figure 6: Examples of 'global failures' of cerebellar parcellation. (A) Sagittal slice ($x= 0$) and coronal slice ($y= -57$) showing a parcellation failure. Here, the cerebellum is only partly segmented, and parts of the occipital lobe have incorrectly been labeled as the cerebellum. These types of failures are likely due to a problem with the header of the original image, which will affect the ACAPULCO affine transformation of the image into world coordinate and subsequent localization of the cerebellum. (B) Sagittal slice ($x= 0$) and coronal slice ($x= -57$) showing a parcellation failure in a person with FRDA. Here, the CM has been completely mis-segmented. The algorithm has labeled the CM at the back of the head (red oval), outside the brain. The boundaries of the white matter have not been captured and are mislabeled as grey matter, particularly affecting left lobules VIIIb and IX. Left lobule X has also been missed (red arrow on coronal slice). These examples warrant immediate exclusion from group-level analyses for ACAPULCO and SUIT analyses. Abbreviations: CM = corpus medullare; Ver = vermis; L/R = left/right. [Please click here to view a larger version of this figure.](#)

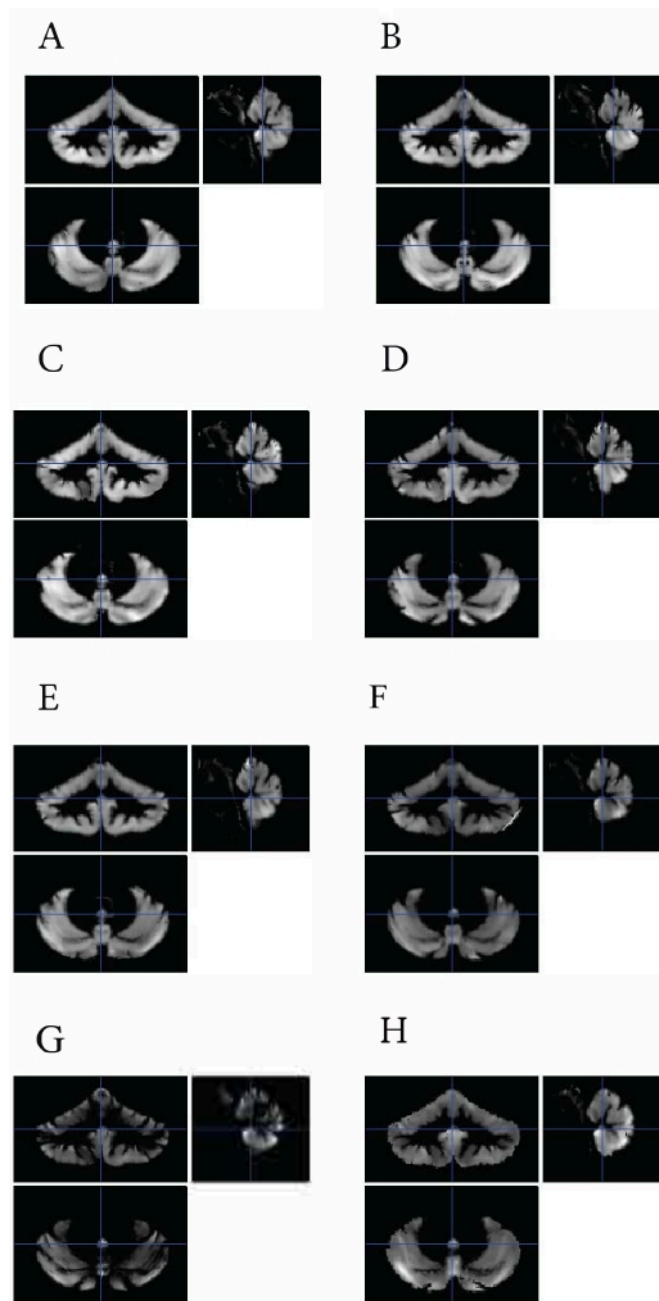


Figure 7: Warped and modulated voxel-based morphometry maps. (A, B) Well-aligned cerebellar grey matter from two HCs. (C) A cerebellum from an HC that was detected as a statistical outlier but was retained in the analysis. (D) An atrophied cerebellum from a person with FRDA. The cerebellum has been warped correctly to the template; hence, this would not warrant exclusion. (E) An exclusion. There is a gradient in contrast from the top to the bottom of the image that reflects an error in the processing. (F) A hyperintense plane artifact in the lower right of the image of unknown origin necessitates exclusion. (G) An example of a heavily atrophied cerebellar of an SCA2 patient. The cerebellum has been warped correctly

to the template; however, there is a lot of missing tissue, resulting in low contrast. This would not be an exclusion. (H) Example of poor masking necessitating exclusion. Abbreviations: VBM = voxel-based morphometry; HC = healthy control; FRDA = Friedreich ataxia; SCA2 = Spinocerebellar ataxia 2. [Please click here to view a larger version of this figure.](#)

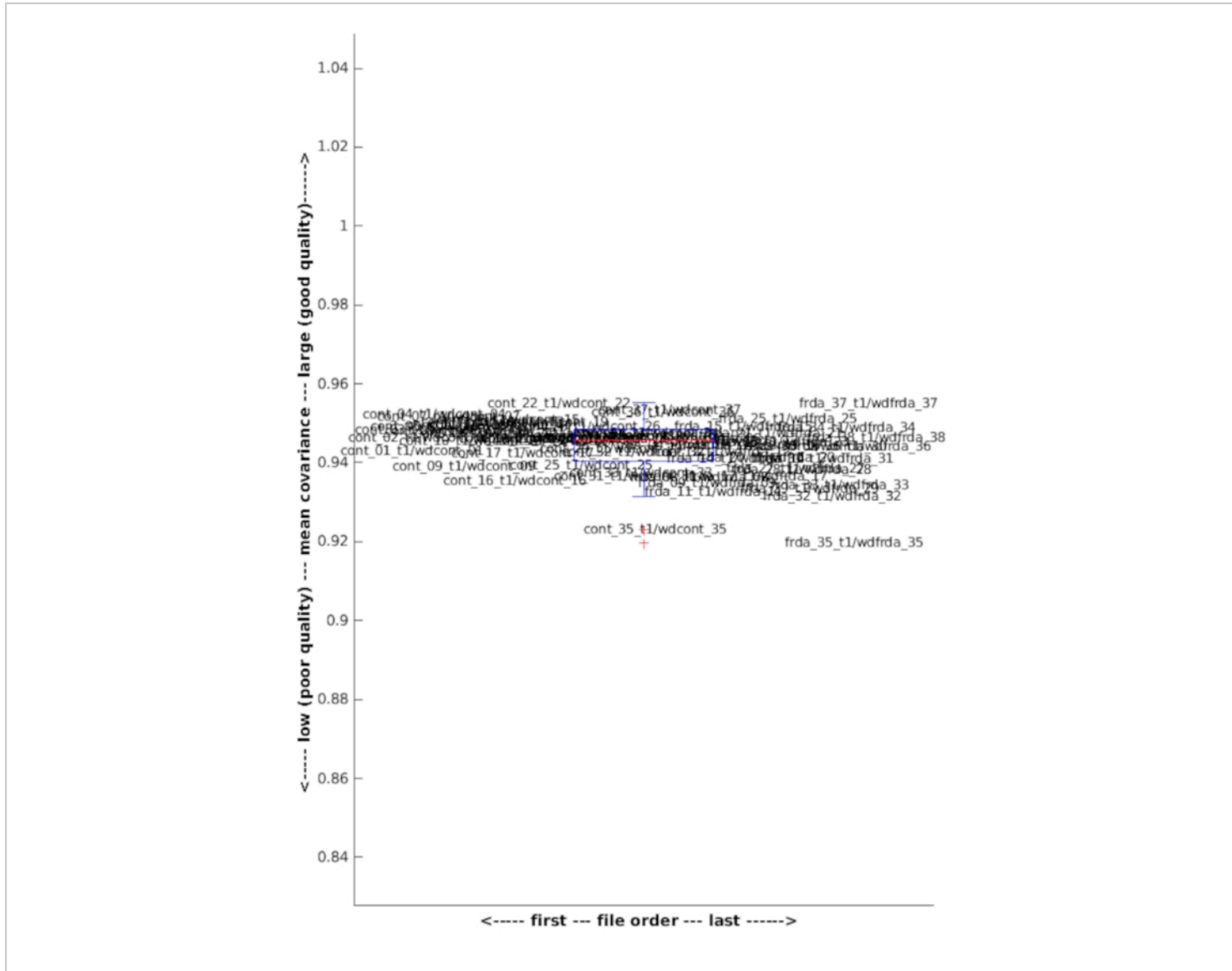


Figure 8: Spatial covariance of SUIT voxel-based morphometry maps. Box plot illustrating the spatial covariance of the voxel-based morphometry maps for a cohort of 64 (28 FRDA) subjects. Spatial covariance is a measure of how well aligned each image is, relative to every other image in the sample. The data are tightly clustered together with an average spatial covariance correlation of ~ 0.95 . Here, two outliers (1 FRDA, 1 HC) were detected, as >2 SDs below the mean. Abbreviations: FRDA = Friedreich ataxia; HC = healthy control; SD = standard deviation; cont = control. [Please click here to view a larger version of this figure.](#)

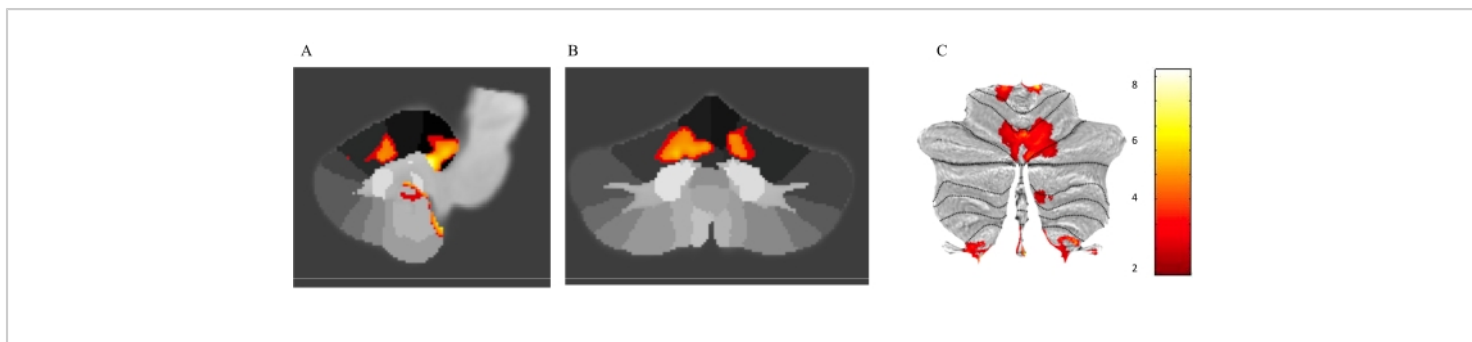


Figure 9. Between-group results of a voxel-based morphometry analysis of cerebellar grey matter morphometry. (A) Sagittal, (B) coronal, and (C) salt map representations of voxel-level statistical maps in individuals with FRDA vs. controls, controlling for ICV. Only voxels that survive $p < 0.05$ FWE cluster-level corrected, are shown. Color bar indicates T statistic. Abbreviations: FRDA = Friedreich ataxia; ICV = intracranial volume; FWE = family-wise error. [Please click here to view a larger version of this figure.](#)

Lobule	% excluded
CM	1.5
Left Crus I	2.9
Left Crus II	2.9
Left I III	2.9
Left IV	1.5
Left IX	4.51
Left V	2.9
Left VI	1.5
Left VIIB	1.5
Left VIIIA	1.5
Left VIIIB	2.9
Left X	2.9
Right Crus I	6.02
Right Crus II	2.9
Right I III	2.9
Right IV	1.5
Right IX	2.9
Right V	1.5
Right VI	1.5
Right VIIB	1.5
Right VIIIA	2.9
Right VIIIB	1.5
Right X	1.5
Vermis IX	1.5
Vermis VI	2.9
Vermis VII	1.5

Vermis VIII	1.5
Vermis X	1.5

Table 1: Cerebellar anatomical lobules derived from ACAPULCO and rates of exclusion (%) across a sample of 31 people with FRDA and 37 HCs. Abbreviations: FRDA = Friedreich ataxia; HC = healthy controls.

Supplemental Table S1: Volumes (mm³) of 28 cerebellar anatomical lobules in Friedreich Ataxia and healthy control individuals. [Please click here to download this Table.](#)

Discussion

The cerebellum is critical to a wide range of human motor³, cognitive⁵⁸, affective¹⁰, and language^{7,59} functions and is implicated in many neurological and psychiatric diseases. The availability of a standardized and easily implementable approach for the quantification of regional cerebellar volumes will contribute to increasingly detailed 'whole-brain' structure-function mapping, complete disease modeling, and improved opportunities to define and track cerebellar contributions to brain diseases. This standardized pipeline described here combines state-of-the-art approaches for automatic cerebellum parcellation and finer-grained spatial profiling of cerebellar grey matter morphometry in both health and disease.

The results of the cross-sectional cerebellum parcellation analysis using ACAPULCO presented here showed that people with FRDA (vs. HC) had significantly reduced white matter volumes. These findings support previous studies of FRDA, which consistently show early, robust, and progressive white matter volume loss, particularly in the dentate nuclei, in FRDA. Furthermore, the pattern and extent of progressive neurodegeneration in the superior and inferior cerebellar peduncles and the dentate nuclei have been shown to differ

as a factor of onset age of FRDA⁴⁴. The results from the SUIT analysis revealed additional findings. Specifically, there was significant voxel-level volume loss in FRDA (vs. HC) in anterior lobe regions corresponding to bilateral lobules I-IV and Right V, extending into lobule VI. In addition, the SUIT analysis revealed significant volume loss in FRDA (vs. HC) in the medial posterior lobe regions, including lobule IX, X, and Vermis. This pattern of between-group differences is comparable to previously published work in the same cohort of FRDA patients, using a whole-brain VBM approach⁵⁵.

Defining cerebellar abnormalities in neurological and psychiatric diseases is a high-priority research area with translational impact. Instrumental to tracking and treating neurological diseases-particularly those where the cerebellum is a primary site of neurodegeneration-is the development of complete biological characterizations of cerebellum involvement. The pipeline presented herein allows for relationships between individual cerebellar lobule grey matter morphometry and clinical measures that are used as the "gold standard" for clinical endpoints of disease to be explored. Such research can have a significant translational impact. For example, in the rare cerebellar diseases space, the identification of a particular profile of cerebellar grey matter atrophy in a subgroup of patients that maps onto or predicts clinical symptoms would have implications for guiding clinical practice. The inclusion of the SUIT module further allows for interesting research questions to be addressed such as structure-function mapping of

the cerebellum or analysis of functional gradients of the cerebellum⁶⁰.

General recommendations for group-level statistical analyses

ACAPULCO: Volumes of each cerebellar lobule (in mm³) for each subject are recorded in *Cerebel_vols.csv*. During statistical inference of group-level effects, intracranial volume (ICV; also recorded in *Cerebel_vols.csv*) should be controlled for to account for variability in head size. Alpha-significance thresholds should be corrected to account for inference across multiple lobules.

SUIT: Grey matter cerebellar VBM can be performed on the `wd<subject>seg1.nii` images using standard MRI processing software such as SPM or FSL. See the CAT12 manual for an excellent introduction to VBM using SPM12⁵⁴. ICV should be controlled for to account for variability in head size.

For VBM in the cerebellum, it is generally recommended to use a Gaussian spatial smoothing kernel of no more than 3 mm full width at half maximum (FWHM). Appropriate statistical correction must be applied to account for multiple comparisons across voxels. In general, it is recommended to use nonparametric approaches (e.g., SnPM or FSL-Randomise).

The most critical step for successful parcellation of the cerebellum using ACAPULCO is general quality-checking of the T1 images **prior to and** post processing. It is highly recommended that the user check for bad contrast images (e.g., an inconsistent gradient across the image) and severe tilting of the head and motion artifacts, all of which can affect the performance of the algorithm. In addition, while the ACAPULCO algorithm has been trained on atrophied cerebellar, it has not been trained on lesion data. It is

anticipated that lesions in the cerebral cortex would not be expected to impact the performance of the algorithm and subsequent accuracy of the parcellation; however, large infarcts in the cerebellum would likely yield parcellation errors. Quality-checking the cerebellum mask post processing is **essential**. Minor parcellation errors (e.g., minor under- and overinclusions of cerebellum lobules) are sometimes not detected as statistical outliers; conversely, instances of incorrect nonoutliers can occur where data are within the normal range, despite an obvious parcellation error. If a subject is identified as an outlier, it is essential to perform follow-up, detailed quality-checking of the cerebellum mask slice-by-slice to guide decision-making about whether to include or exclude the lobule(s) for that subject. Another critical step when running the SUIT pipeline (Module 2) is that it requires the ACAPULCO module to have already been run. Specifically, SUIT requires the cerebellum mask produced in ACAPULCO to run the cerebellum isolation and segmentation. It is important that the cerebellum mask is quality-checked to ensure full cerebellar coverage.

There are some limitations to the protocol. First, while ACAPULCO achieves state-of-the-art accuracy for cerebellar grey matter parcellation, it is not optimized for white matter parcellation; the corpus medullare covers the main body of the white matter but does not provide a measure of all the white matter. Second, the convolutional neural networks used to localize and segment the cerebellum in ACAPULCO do not generalize well to images with different contrasts or images that were not used in training. For example, because only 3T images were used in training, the parcellation quality using images acquired on a 1.5 T scanner is typically not as good; furthermore, there are no statistics with respect to ground truth that has been performed on these images. Finally, the pipeline controls for the confounding effects of head size on

cerebellum volume estimates by providing an estimate of ICV that can be included as a regressor of no interest in group-level statistical analyses. However, an ideal approach would be to calculate ICV-corrected cerebellum volumes at the individual level prior to running QC, such that detected outliers reflect a true parcellation error and not natural variability in the subjects' neuroanatomy (e.g., having a large head).

In conclusion, we present a standardized pipeline for examining cerebellum grey mater morphometry, which has broad applicability to a range of neurological diseases. The pipeline is set up to allow for large, multisite studies and 'mega analyses' and is publicly available for use by research groups to facilitate reliability and reproducibility across the field. Ultimately, this pipeline provides a powerful methodological approach for further characterizing and tracking cerebellar structural changes with disease progression in neurological diseases. A longitudinal pipeline is currently being developed.

Disclosures

The authors have no conflicts of interest to disclose.

Acknowledgments

The work presented in this manuscript was funded by an Australian National Health and Medical Research Council (NHMRC) Ideas Grant: APP1184403.

References

1. Holmes, G. The cerebellum of man (Hughlings Jackson memorial lecture). *Brain*. **62**, 1-30 (1939).
2. Ito, M. The modifiable neuronal network of the cerebellum. *The Japanese Journal of Physiology*. **34** (5), 781-792 (1984).
3. Manto, M., Oulad Ben Taib, N. The contributions of the cerebellum in sensorimotor control: what are the prevailing opinions which will guide forthcoming studies? *Cerebellum*. **12** (3), 313-315 (2013).
4. Manto, M., Gandini, J., Feil, K., Strupp, M. Cerebellar ataxias: an update. *Current Opinion in Neurology*. **33** (1), 150-160 (2020).
5. Schmahmann, J. D. Disorders of the cerebellum: ataxia, dysmetria of thought, and the cerebellar cognitive affective syndrome. *The Journal of Neuropsychiatry and Clinical Neurosciences*. **16** (3), 367-378 (2004).
6. Strick, P. L., Dum, R. P., Fiez, J. A. Cerebellum and nonmotor function. *Annual Review of Neuroscience*. **32**, 413-434 (2009).
7. King, M., Hernandez-Castillo, C. R., Poldrack, R. A., Ivry, R. B., Diedrichsen, J. Functional boundaries in the human cerebellum revealed by a multi-domain task battery. *Nature Neuroscience*. **22** (8), 1371-1378 (2019).
8. Schmahmann, J. D. An emerging concept. The cerebellar contribution to higher function. *Archives of Neurology*. **48** (11), 1178-1187 (1991).
9. Schmahmann, J. D., Sherman, J. C. The cerebellar cognitive affective syndrome. *Brain*. **121** (Pt 4), 561-579 (1998).
10. Schutter, D. J., van Honk, J. The cerebellum on the rise in human emotion. *Cerebellum*. **4** (4), 290-294 (2005).
11. Stoodley, C. J., Schmahmann, J. D. Functional topography in the human cerebellum: a meta-analysis of neuroimaging studies. *Neuroimage*. **44** (2), 489-501 (2009).
12. Guell, X., Gabrieli, J. D. E., Schmahmann, J. D. Triple representation of language, working memory, social

- and emotion processing in the cerebellum: convergent evidence from task and seed-based resting-state fMRI analyses in a single large cohort. *Neuroimage*. **172**, 437-449 (2018).
13. Lewis, M. M. et al. The role of the cerebellum in the pathophysiology of Parkinson's disease. *The Canadian Journal of Neurological Sciences*. **40** (3), 299-306 (2013).
 14. Möller, C. et al. Different patterns of gray matter atrophy in early- and late-onset Alzheimer's disease. *Neurobiology of Aging*. **34** (8), 2014-2022 (2013).
 15. Colloby, S. J., O'Brien, J. T., Taylor, J. P. Patterns of cerebellar volume loss in dementia with Lewy bodies and Alzheimer's disease: A VBM-DARTEL study. *Psychiatry Research*. **223** (3), 187-191 (2014).
 16. McDonald, C. R. et al. Subcortical and cerebellar atrophy in mesial temporal lobe epilepsy revealed by automatic segmentation. *Epilepsy Research*. **79** (2-3), 130-138 (2008).
 17. Marcián, V. et al. Morphological changes of cerebellar substructures in temporal lobe epilepsy: A complex phenomenon, not mere atrophy. *Seizure*. **54**, 51-57 (2018).
 18. Nopoulos, P. C., Ceilley, J. W., Gailis, E. A., Andreasen, N. C. An MRI study of cerebellar vermis morphology in patients with schizophrenia: evidence in support of the cognitive dysmetria concept. *Biological Psychiatry*. **46** (5), 703-711 (1999).
 19. Stoodley, C. J. Distinct regions of the cerebellum show gray matter decreases in autism, ADHD, and developmental dyslexia. *Frontiers in Systems Neuroscience*. **8**, 92 (2014).
 20. Larsell, O. The development of the cerebellum in man in relation to its comparative anatomy. *The Journal of Comparative Neurology*. **87** (2), 85-129 (1947).
 21. Haines, D. E., Mihailoff, G. A. The Cerebellum. in *Fundamental neuroscience for basic and clinical applications*. 5th edn, Elsevier, 394-412 (2018).
 22. Kelly, R. M., Strick, P. L. Cerebellar loops with motor cortex and prefrontal cortex of a nonhuman primate. *Journal of Neuroscience*. **23** (23), 8432-8444 (2003).
 23. Schmahmann, J. D., Pandya, D. N. Anatomical investigation of projections to the basis pontis from posterior parietal association cortices in rhesus monkey. *The Journal of Comparative Neurology*. **289** (1), 53-73 (1989).
 24. Buckner, R. L., Krienen, F. M., Castellanos, A., Diaz, J. C., Yeo, B. T. The organization of the human cerebellum estimated by intrinsic functional connectivity. *Journal of Neurophysiology*. **106** (5), 2322-2345 (2011).
 25. Fischl, B. FreeSurfer. *Neuroimage*. **62** (2), 774-781 (2012).
 26. Shattuck, D. W., Leahy, R. M. BrainSuite: an automated cortical surface identification tool. *Medical Image Analysis*. **6** (2), 129-142 (2002).
 27. Patenaude, B., Smith, S. M., Kennedy, D. N., Jenkinson, M. A Bayesian model of shape and appearance for subcortical brain segmentation. *Neuroimage*. **56** (3), 907-922 (2011).
 28. Bogovic, J. A., Bazin, P. L., Ying, S. H., Prince, J. L. Automated segmentation of the cerebellar lobules using boundary specific classification and evolution. *Information Processing in Medical Imaging*. **23**, 62-73 (2013).

29. Bogovic, J. A., Prince, J. L., Bazin, P. L. A Multiple object geometric deformable model for image segmentation. *Computer Vision and Image Understanding: CVIU*. **117** (2), 145-157 (2013).
30. Price, M., Cardenas, V. A., Fein, G. Automated MRI cerebellar size measurements using active appearance modeling. *Neuroimage*. **103**, 511-521 (2014).
31. Chakravarty, M. M. et al. Performing label-fusion-based segmentation using multiple automatically generated templates. *Human Brain Mapping*. **34** (10), 2635-2654 (2013).
32. Weier, K., Fonov, V., Lavoie, K., Doyon, J., Collins, D. L. Rapid automatic segmentation of the human cerebellum and its lobules (RASCAL)--implementation and application of the patch-based label-fusion technique with a template library to segment the human cerebellum. *Human Brain Mapping*. **35** (10), 5026-5039 (2014).
33. Yang, Z. et al. Automated cerebellar lobule segmentation with application to cerebellar structural analysis in cerebellar disease. *Neuroimage*. **127**, 435-444 (2016).
34. Romero, J. E. et al. CERES: A new cerebellum lobule segmentation method. *Neuroimage*. **147**, 916-924 (2017).
35. Carass, A. et al. Comparing fully automated state-of-the-art cerebellum parcellation from magnetic resonance images. *Neuroimage*. **183**, 150-172 (2018).
36. Han, S., Carass, A., He, Y., Prince, J. L. Automatic cerebellum anatomical parcellation using U-Net with locally constrained optimization. *Neuroimage*. **218**, 116819 (2020).
37. Ashburner, J., Friston, K. J. Voxel-based morphometry--the methods. *Neuroimage*. **11** (6 Pt 1), 805-821 (2000).
38. Jenkinson, M., Smith, S. A global optimisation method for robust affine registration of brain images. *Medical Image Analysis*. **5** (2), 143-156 (2001).
39. Andersson, J., Jenkinson, M., Smith, S. Non-linear registration, aka spatial normalisation. Report No. TR07JA2 (2010).
40. Ashburner, J., Friston, K. J. Unified segmentation. *Neuroimage*. **26** (3), 839-851 (2005).
41. Dahnke, R., Yotter, R. A., Gaser, C. Cortical thickness and central surface estimation. *Neuroimage*. **65**, 336-348 (2013).
42. Diedrichsen, J. A spatially unbiased atlas template of the human cerebellum. *Neuroimage*. **33** (1), 127-138 (2006).
43. Diedrichsen, J., Balsters, J. H., Flavell, J., Cussans, E., Ramnani, N. A probabilistic MR atlas of the human cerebellum. *Neuroimage*. **46** (1), 39-46 (2009).
44. Harding, I. H. et al. Brain structure and degeneration staging in Friedreich ataxia: Magnetic resonance imaging volumetrics from the ENIGMA-Ataxia Working Group. *Annals of Neurology*. **90** (4), 570-583 (2021).
45. Enigma. Structural imaging processing protocols. <http://enigma.ini.usc.edu/protocols/imaging-protocols/> (2021).
46. Poldrack Lab, Stanford University. MRIQC. <https://mriqc.readthedocs.io/en/stable/> (2020).
47. Rorden Lab, University of South Carolina. dcm2niix. <https://github.com/rordenlab/dcm2niix> (2021).
48. Docker. <https://docs.docker.com/> (2021).
49. Sylabs. Singularity. <https://sylabs.io/singularity> (2021).
50. The MathWorks, Inc. MATLAB. <https://au.mathworks.com/> (2021).

51. The Wellcome Centre for Human Neuroimaging. Statistical parametric mapping SPM12. <https://www.fil.ion.ucl.ac.uk/spm/software/spm12/> (2020).
52. Diedrichsen Lab, University of Western Ontario. <http://www.diedrichsenlab.org/imaging/suit.htm>
53. FreeSurfer download and install. <https://surfer.nmr.mgh.harvard.edu/fswiki/DownloadAndInstall> (2020).
54. Gaser, C., Dahnke, R. CAT: A computational anatomy toolbox for SPM. <http://www.neuro.uni-jena.de/cat/> (2020).
55. Selvadurai, L. P. et al. Cerebral and cerebellar grey matter atrophy in Friedreich ataxia: the IMAGE-FRDA study. *Journal of Neurology*. **263** (11), 2215-2223 (2016).
56. Schmahmann, J. D. The cerebellum and cognition. *Neuroscience Letters*. **688**, 62-75 (2019).
57. Diedrichsen, J., Zotow, E. Surface-based display of volume-averaged cerebellar imaging data. *PLoS One*. **10**(7), e0133402 (2015).
58. Gottwald, B., Mihajlovic, Z., Wilde, B., Mehdorn, H. M. Does the cerebellum contribute to specific aspects of attention? *Neuropsychologia*. **41** (11), 1452-1460 (2003).
59. Starowicz-Filip, A. et al. The role of the cerebellum in the regulation of language functions. *Psychiatria Polska*. **51** (4), 661-671 (2017).
60. Guell, X., Schmahmann, J. D., Gabrieli, J., Ghosh, S. S. Functional gradients of the cerebellum. *Elife*. **7**, e36652 (2018).